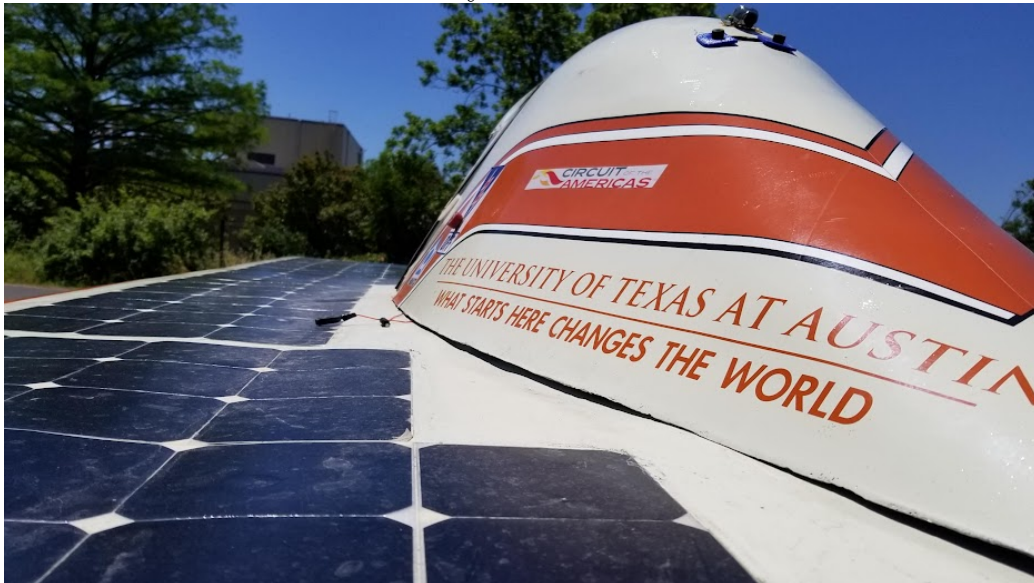


Evaluation and Improvement of Photovoltaic Power Systems

The University of Texas at Austin



Matthew Junkit Yu

17 December 2022

Contents

1	Introduction	5
2	Modeling Photovoltaics	8
2.1	Three Parameter Solar Cell Model	9
2.1.1	Model Introduction	9
2.1.2	Photocurrent	10
2.1.3	Dark Current	11
2.1.4	Dark Saturation Current	12
2.1.5	Short Circuit Current	13
2.1.6	Open Circuit Voltage	15
2.1.7	Model Summary	17
2.2	Five Parameter Solar Cell Model	19
2.2.1	Model Introduction	19
2.2.2	Shunt Resistance	19
2.2.3	Series Resistance	20
2.2.4	Photocurrent as a Ratio of Shunt/Series Resistance . .	22
2.2.5	Shunt and Series Resistance as a Function of Irradi- ance, Temperature	24
2.2.6	Model Summary	27
2.3	Seven Parameter Solar Cell Model	29
2.4	Evaluation of Solar Cell Models	30
2.4.1	Solar Cell Dataset	30
2.4.2	Methods to Fit Cells	30
2.5	Modeling Solar Modules	31
2.6	Evaluation of Solar Module Models	32
2.7	Modeling Solar Arrays	33
2.8	Evaluation of Solar Array Models	34

3	Optimizing Photovoltaics	35
4	Optimizing Photovoltaic Systems	36
5	Conclusion	37
	Bibliography	38
	Appendices	41
A	Acronyms and Abbreviations	42
B	Mathematical Nomenclature	43
C	Iterative Solvers for the Five Parameter Solar Cell Model	45
D	Measurement of Parasitic Resistances	46

List of Figures

2.1	Three Parameter, or Single Diode Model of a Solar Cell	9
2.2	Maxeon Gen III Cell Spectral Response	11
2.3	Solar Cell Temperature Dependence	14
2.4	Solar Cell Irradiance Dependence	15
2.5	Five Parameter, or Full Single Diode Model of a Solar Cell . .	19
2.6	Effect of Series (a) and Shunt Resistance (b) on current-voltage (I-V) Curve	20
2.7	Current Flow Junction of Five Parameter Model Solar Cell . .	21
2.8	Shunt Resistance vs Temperature [5]	24
2.9	Shunt Resistance vs Irradiance [5]	25
2.10	Series Resistance vs Temperature [5]	25
2.11	Series Resistance vs Irradiance [5]	26
2.12	Solar Cell With Varying Series Resistances [13]	27
2.13	Seven Parameter, or Double Diode Model of a Solar Cell . . .	29

List of Tables

2.1	Various Ideality Factors of ideality factor (n)	12
2.2	Dark Current Ratios for Various Reference Cells	22

Chapter 1

Introduction

In order to reach net zero emissions targets set by the United Nations (UN) at the 2015 Paris Agreement [16] before 2050, the International Energy Association (IEA) estimates that nearly 630 Gigawatts (GW) [15] of photovoltaic (PV) energy generation capacity need to be added annually by 2030. As of 2022, we observed that at least 175 GW were installed in 2021 [12] [11], a 22% year over year growth. With large policy and geopolitical tailwinds behind major economies like the United States and Europe, solar is expected to be one of the, if not the major driver of new energy generation within the next two decades.

However, in order to achieve this target generation capacity in a sustainable way, engineers and PV designers need to maximize the electrical efficiency of the overall power system, as opposed to just improving the solar cell efficiency. According to the U.S. Energy Information Administration (EIA) [18], the capacity factor of PVs as an energy source in the United States reached a monthly maximum of 33.4% in June of 2022; *capacity factor* is defined by the EIA as a measure of the generated output by the electric generator versus the maximum possible output. It is clear that system inefficiencies in PV generation provide large constraints, and optimistically, equally large opportunities, in allowing us to increase our pace towards reaching net zero carbon emissions by 2050.

This thesis takes a holistic evaluation of the PV power generation system in a unique use case that necessitates maximizing the capacity factor: solar powered vehicles. We evaluate the modeling, creation, and optimization of a solar powered vehicle for the University of Texas at Austin’s Longhorn Racing Solar (LHRs) team, and attempt to identify and address inefficiencies and

bottlenecks whose improvements will help the larger **PV** industry as a whole.

In particular, this thesis will focus on three important and active areas of development within the **PV** field: solar array modeling and prediction, solar cell binning processes and heuristics, and maximum power point tracking (**MPPT**) algorithms. In each of these areas, we look at the state of the art techniques, propose novel ideas to improve our understanding of the system and its inefficiencies, and see if we can translate it lateral applications like rooftop solar or industrial **PV**. Note that in this thesis we refer to photovoltaics and solar without distinction.

In the first major chapter, **Modeling Photovoltaics**, this thesis discusses how can solar cells can be modeled at various abstraction layers, from idealized cells at standard conditions using the 3-parameter model to non-idealized cells that incorporate parasitic resistances using the 7-parameter model. These solar cell models are then evaluated against a dataset of several hundred solar cell **I-V** and power-voltage (**P-V**) curves generated from our custom testing setup to see how well the model fits real cells at different conditions. We build upon these models to form larger units of **PVs**, such as solar modules and solar arrays, which may consist of strings of cells in series with bypass diodes across them, among other configurations. Some important topics that are explored using these multi-cell models include **PV** mismatch and bypass activation. Insights from these topics lead to heuristics that are proposed in the next chapter, **Optimizing Photovoltaics**.

The second major chapter, **Optimizing Photovoltaics**, takes the aforementioned models and dataset created to propose a process to bin, match, and combine solar cells and modules, with the end goal of maximizing the performance of the solar array that will be attached to the solar vehicle. In this chapter, we propose design criteria, heuristics, and methodologies to generate designs for the solar vehicle that fit the unique constraints of the application, which center around the dynamism of the system as it moves in transit across the real world.

In the third and final major chapter, **Optimizing Photovoltaic Systems**, this thesis investigates the operation of the **PV** system in the context of the solar vehicle. We observe the energy conversion process from incident light on the solar array to electricity captured by the battery protection system (**BPS**) and present a **PV** system simulator and a suite of **MPPT** algorithms to minimize energy losses from the aforementioned conversion process. We demonstrate custom hardware developed by the **LHRs** team and evaluate in real world settings a select set of **MPPT** algorithms. We compare

The second area of development may be more generalized then this.

these results with existing research and our digital twin model of the solar vehicle, and finally discuss conclusions from the three chapters that can be translatable to the wider **PV** industry.

Along with these three major chapter, we also provide a large set of appendices corresponding to the development of the main body of work in this thesis. Among them include manufacturing procedures for testing, assembling, and laminating solar cells into solar modules, schematics and accompanying documentation for hardware that was used for characterizing and validating parts of the thesis, software diagrams with relevant open source software repositories developed by our team, and extra insights into the design of the **LHRs**' photovoltaic array that are not directly applicable to the major chapters, such as thermal models performed of the vehicle topshell that influenced our simulation models, among others.

Chapter 2

Modeling Photovoltaics

Insert intro paragraph on the focus of this chapter, as well as the a short discussion of the following sections.

2.1 Three Parameter Solar Cell Model

2.1.1 Model Introduction

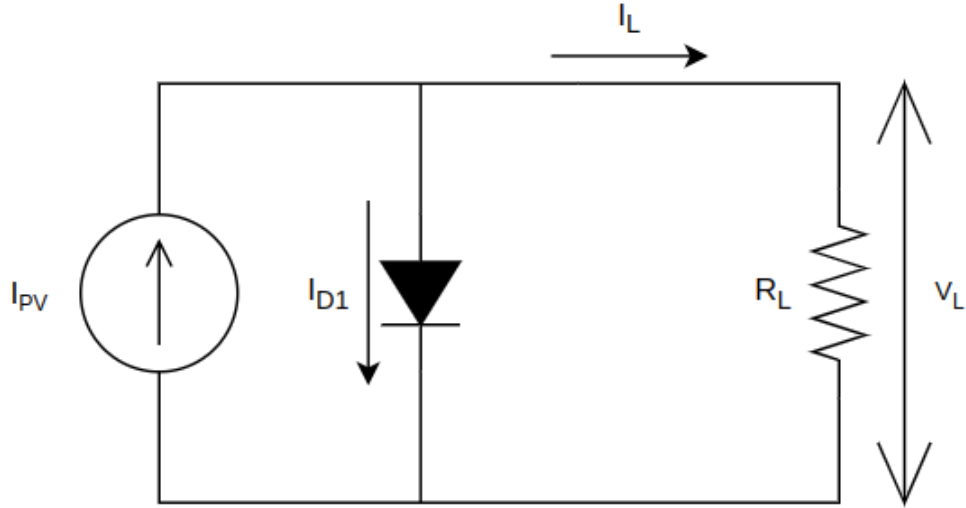


Figure 2.1: Three Parameter, or Single Diode Model of a Solar Cell

The most basic model of a solar cell is the three parameter model, or single diode model, shown in Figure 2.1. It consists of a constant current source and a diode. The constant current source produces a photocurrent, or light generated current (I_{PV}) caused by photons of sufficient energy being absorbed into the surface of the solar cell and exciting charge carriers (generally in the form of electrons) to enter the circuit. The diode represents the various recombination processes that consume the generated current in the form of dark current, or diode current (I_D).

In this model, the three parameters consist of the following:

- the photocurrent I_{PV} ,
- a dark saturation current, or reverse saturation current (I_0),
- and an n .

The latter two are contained within the dark current I_D , and generally influence the shape of the predicted I - V curve, particularly around the knee-bend.

This model is juxtaposed from the five parameter model in that it does not incorporate cell losses in the form of series resistance (R_S) and shunt resistance (R_{SH}). It is assumed that the series resistance is zero (short circuit) and the shunt resistance is infinite (open circuit). The five parameter model may also be called the complete single diode model.

We observe from Figure 2.1 that the load current (I_L) can be represented as a function of the photocurrent I_{PV} and the dark current I_D , shown in Equation 2.1.

$$I_L = I_{PV} - I_D \quad (\text{A}) \quad (2.1)$$

In the following subsections, we break down each component into its constituent parts.

2.1.2 Photocurrent

$$I_{PV} = qA \int b_s(E)QE(E)dE \quad (\text{A}) \quad (2.2)$$

On a fundamental level, we can define the photocurrent I_{PV} as a function of the photons incident upon the surface of the solar cell and the solar cell's spectral response. This is demonstrated in Equation 2.2. A bulleted explanation of this equation oriented for the layman is as follows:

- Incident light hits the solar cell over a given spectrum of energy levels (denoted either in eV or in nm) (see Figure 2.2).
- Incident light at each discrete energy level has an spectral photon flux density ($b_s(E)$), otherwise known as intensity.
- The solar cell has a given quantum efficiency ($QE(E)$) at each energy level, which is the probability that an incident photon of energy (E) delivers one electron to the external circuit.
- Integrating the product of the photon flux density $b_s(E)$ and quantum efficiency $QE(E)$ (then multiplied by the electric charge constant (q) and the cell area (A)) provides the photocurrent I_{PV} .

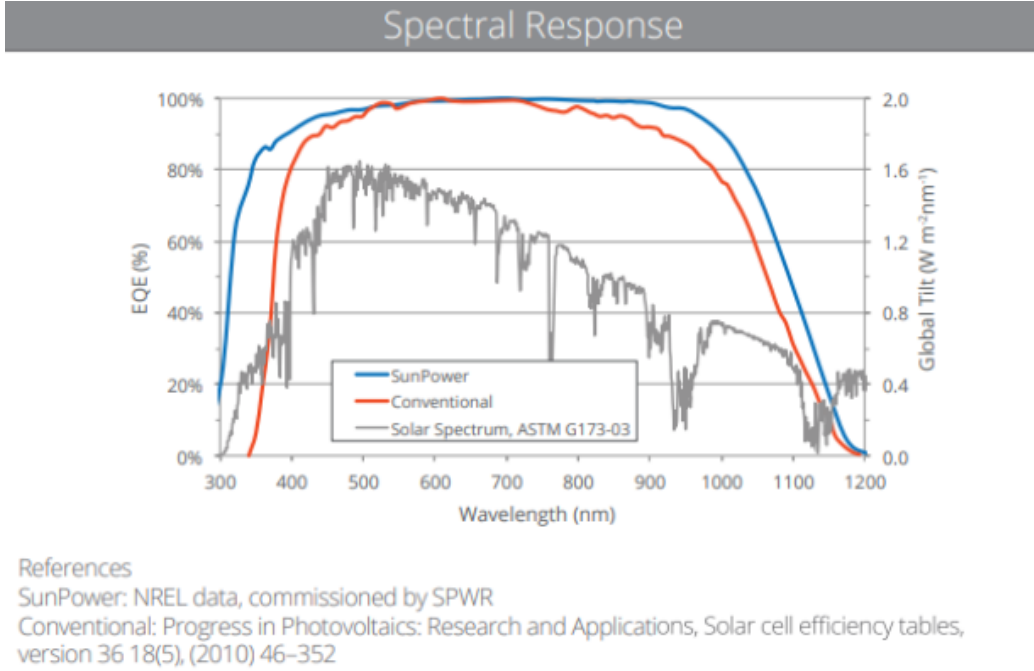


Figure 2.2: Maxeon Gen III Cell Spectral Response

Solar cell manufacturers may provide a spectral response chart showing the quantum efficiency over the useful solar spectrum (as seen in Figure 2.2), but will generally just provide the short circuit current (I_{SC}) at standard test conditions (STC) (1000 W m^{-2} , $AM\ 1.5G$, $25\text{ }^{\circ}C$).

As it turns out, the photocurrent I_{PV} can generally be approximated as the short circuit current I_{SC} .

$$I_{PV} = I_{SC} \quad (\text{A}) \quad (2.3)$$

We'll discuss in Section 2.2.3 that Cubas et al. [3][4] defines the photocurrent as a ratio of the series and shunt resistance in addition to the short circuit current. However, in most cases, the empirical value of I_{SC} will not differ from Equation 2.3.

2.1.3 Dark Current

The dark current I_D comprises of the interesting and critical parameters of the three parameter model; shown in Equation 2.4, it consists of the term I_0

and an exponential. The exponential is a function of three key variables: the cell temperature (T_C), load voltage (V_L), and ideality factor n .

This ideality factor is typically between 1 and 2, and represents the proportional influence of carriers in several recombination processes for a given cell composition and structure. Some ideality factor values are presented in Table 2.1, sourced from PVEducation’s Ideality Factor page [8]. We note that the ideality factor may be outside the typical range of $[1, 2]$, as discussed by Jain et Kapoor [9] and R.N. Hall [6], the latter of which notes that Auger recombination dominated dark currents generate a n of $2/3$.

The term thermal voltage (V_T) which encapsulates the T_C dependency describes the voltage across the P-N junction of the diode in the model: at STC this is typically 26 mV . It is defined by Equation 2.5.

$$I_D = I_0[\exp(\frac{V}{V_T}) - 1] \quad (\text{A}) \quad (2.4)$$

$$V_T = \frac{nk_B T_C}{q} \quad (\text{V}) \quad (2.5)$$

Recombination Type	Ideality Factor	Description
SRH, band to band (low level injection)	1	Recombination limited by minority carrier.
SRH, band to band (high level injection)	2	Recombination limited by both carrier types.
Auger	$2/3$	Two majority and one minority carriers required for recombination.
Depletion region (junction)	2	Two carriers limit recombination.

Table 2.1: Various Ideality Factors of n

2.1.4 Dark Saturation Current

The dark saturation current I_0 has two potential derivations. Generally, the three parameter model, (see Baig et al. [1], MacAlpine et Brandemuehl [10], Rusirawan et Farkas [17], and others) define I_0 as in Figure 2.6; where the

diode current is a function of the cell temperature and the energy bandgap in relation to several reference parameters at **STC**.

$$I_0 = I_{0,ref} \left(\frac{T_C}{T_{C,ref}} \right)^3 \exp \left(\frac{E_{G,ref}}{k_B T_{C,ref}} - \frac{E_G}{k_B T_C} \right) \quad (\text{A}) \quad (2.6)$$

On the other hand, we can derive the I_0 algebraically: given the short circuit current I_{SC} and open circuit voltage (V_{OC}), we can set the cell at open circuit, forming the derivation in Equation 2.7 and the result in Equation 2.8.

$$\begin{aligned} I_L &= 0 \\ &= I_{SC} - I_D \\ &= I_{SC} - I_0 \left[\exp \left(\frac{V_{OC}}{V_T} \right) - 1 \right] \end{aligned} \quad (\text{A}) \quad (2.7)$$

$$I_0 = I_{SC} \left[\exp \left(\frac{V_{OC}}{V_T} \right) - 1 \right]^{-1} \quad (\text{A}) \quad (2.8)$$

These two competing models of the dark saturation current will be explored further at the end of Chapter 2 in Section 2.4.

2.1.5 Short Circuit Current

Finally, for the three parameter model, we derive the dependence of I_{SC} and V_{OC} on irradiance and temperature before establishing the final derivation of Equation 2.1.

Starting with the short circuit current, it is known that there is a large positive correlation with irradiance and a small positive correlation with temperature, shown in Figures 2.3 and 2.4.

The dependence of irradiance on short circuit current can be modeled as linearly proportional to the light incident upon the solar cell over the reference irradiance. This makes intuitive sense: given half the available light (assuming the distribution of light across the spectrum is consistent), the solar cell will only be able to capture half the maximum available power. Chegaar et al. [2] proposes this relationship as Equation 2.9, where the short circuit current is a function of short circuit current constant (K_E) and irradiance (G) (the latter in units of Wm^{-2}).

$$I_{SC}(G) = K_E G \quad (\text{A}) \quad (2.9)$$

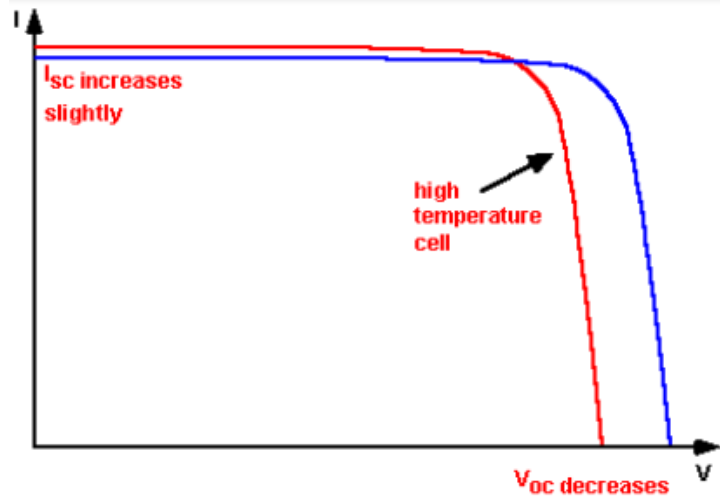


Figure 2.3: Solar Cell Temperature Dependence

Equation 2.9 can be easily reworked where the constant K_E is now based on a reference short circuit current and irradiance, preferably at STC. This forms Equation 2.10, which is the same form used by Baig et al. [1].

$$I_{SC}(G) = I_{SC,ref} \frac{G}{G_{ref}} \quad (\text{A}) \quad (2.10)$$

Hishikawa et al. [7] proposes modeling the dependence of temperature on short circuit current density using a thermal coefficient, α . α is empirically determined given the material composition and structure of the solar cell; for crystalline silicon solar cells, this is approximately 0.05%/K, or 0.0005. Equation 2.11 shows how given α , the change in temperature affects short circuit current density and vice versa. Rearranging the equation leads to the derivation Equation 2.12. This is effectively equivalent to Rusirawan et Farkas [17], but is slightly different from MacAlpine et Brandemuehl [10] and Baig et al. [1], who take the 1 term and replaces it with a another $I_{SC,ref}$, shown in Equation 2.13.

$$\alpha = \frac{1}{I_{SC,ref}} \frac{\Delta I_{SC}}{\Delta T_C} = \frac{1}{I_{SC,ref}} \frac{I_{SC,ref} - I_{SC}}{T_{C,ref} - T_C} \quad (\text{unitless}) \quad (2.11)$$

$$I_{SC}(T_C) = I_{SC,ref} [1 - \alpha(T_{C,ref} - T_C)] \quad (\text{A}) \quad (2.12)$$

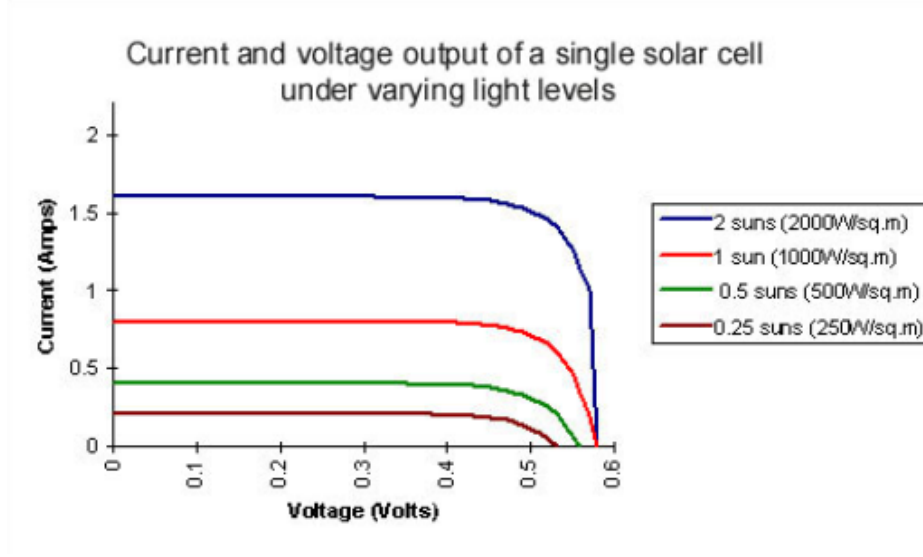


Figure 2.4: Solar Cell Irradiance Dependence

$$I_{SC}(T_C) = I_{SC,ref}[I_{SC,ref} - \alpha(T_{C,ref} - T_C)] \quad (\text{A}) \quad (2.13)$$

These two competing models of the short circuit current will also be explored further at the end of Chapter 2 in Section 2.4. For the purposes of completing this subsection, however, we will combine Equations 2.10 and 2.12 to give us Equation 2.14.

$$I_{SC}(G, T_C) = I_{SC,ref} \frac{G}{G_{ref}} [1 - \alpha(T_{C,ref} - T_C)] \quad (\text{A}) \quad (2.14)$$

2.1.6 Open Circuit Voltage

Likewise, the open circuit voltage is also a function of temperature and irradiance. It is known that the open circuit voltage has a medium positive correlation with irradiance and a medium negative correlation with temperature, shown back in Figures 2.3 and 2.4.

Returning to Equation 2.8, in which we defined the dark saturation current I_0 as a function of the open circuit voltage V_{OC} , we can invert the equation to retrieve the V_{OC} parameter, shown in Equation 2.15.

$$V_{OC} = V_T \ln\left(\frac{I_{SC}}{I_0} + 1\right) \quad (\text{V}) \quad (2.15)$$

There are three points in this equation that can now be determined. We know from Equation 2.5 that the thermal voltage is dependent on the cell temperature T_C . We can also plug in one of the proposed models for I_{SC} . However, we cannot reuse Equation 2.8 because Equation 2.15 was derived from it! Chegaar et al. [2] simplifies the logarithmic term to form Equation 2.16.

$$V_{OC}(G, T_C) = V_{OC,ref} + V_T(T_C) \ln\left(\frac{G}{G_{ref}} + 1\right) \quad (\text{V}) \quad (2.16)$$

This term fits well with the paper's experimental data, but is not immediately clear how it models the original term. It also does not properly model temperature change. Equation 2.17 is a modified form that implements temperature dependence while retaining irradiance dependence.

$$V_{OC}(G, T_C) = V_{OC,ref}[1 - \beta(T_{C,ref} - T_C)] + \frac{nk_B(T_{C,ref} + T_C/\gamma)}{q} \ln\left(\frac{G}{G_{ref}}\right) \quad (\text{V}) \quad (2.17)$$

$$\beta = \frac{1}{V_{OC,ref}} \frac{\Delta V_{OC}}{\Delta T_C} = \frac{1}{V_{OC,ref}} \frac{V_{OC,ref} - V_{OC}}{T_{C,ref} - T_C} \quad (\text{unitless}) \quad (2.18)$$

Equation 2.17 implements two changes: a linear constant β that represents the open circuit voltage temperature coefficient and a modifier T_C/γ . β is likewise empirically determined given the material composition and structure of the solar cell; for silicon it known to be -0.3%/K, or -0.003.

The modifier is an experimentally determined curve fitting term, and may more appropriately model the exponential decrease of V_{OC} at low light conditions. It has an expected operable range of values between [1, 100], where smaller values correlate to a wider range of V_{OC} movement at low light conditions. This parameter, however, is not part of the three parameter cell model. Its efficacy will be explored further at the end of Chapter 2 in Section 2.4.

2.1.7 Model Summary

To conclude this section, we will review the components that make up the three parameter cell model, propose three items of further exploration, and propose a complete model function that incorporates the topics discussed.

Firstly, the three parameter cell model is composed of a constant current source and a power consuming diode, representing photogeneration and recombination effects of the solar cell, respectively. These two components form three parameters that is the namesake of this section, namely the photocurrent, dark saturation current, and ideality factor.

Secondly, we explore the construction and interpretation of these three components, and along the way, examine three areas that deviate from the existing models that we would like to investigate:

- an algebraic derivation of the dark saturation current I_0 ,
- an alternative interpretation of the short circuit current I_{SC} as a function of temperature,
- and a new curve fitting coefficient, γ , to improve open circuit voltage V_{OC} modeling at low lighting conditions.

Finally, we present the complete model function and its derivation, in Equation 2.19.

Reformat
this
equation

$$\begin{aligned}
I_L(V_L, G, T_C) &= I_{PV}(G, T_C) - I_D(V_L, G, T_C) \\
&= I_{SC}(G, T_C) - I_D(V_L, G, T_C) \\
&= I_{SC}(G, T_C) - I_0[\exp(\frac{V_L}{V_T(T_C)}) - 1] \\
&= I_{SC}(G, T_C) - I_{SC}(G, T_C)[\exp(\frac{V_{OC}(G, T_C)}{V_T(T_C)}) - 1]^{-1}[\exp(\frac{V_L}{V_T(T_C)}) - 1] \\
&= I_{SC}(G, T_C) - I_{SC}(G, T_C) \frac{\exp(\frac{V_L}{V_T(T_C)}) - 1}{\exp(\frac{V_{OC}(G, T_C)}{V_T(T_C)}) - 1} \\
&= I_{SC}(G, T_C) - I_{SC}(G, T_C) \frac{\exp(\frac{qV_L}{nk_B T_C}) - 1}{\exp(\frac{qV_{OC}(G, T_C)}{nk_B T_C}) - 1} \\
&= I_{SC}(G, T_C) [1 - \frac{\exp(\frac{qV_L}{nk_B T_C}) - 1}{\exp(\frac{qV_{OC}(G, T_C)}{nk_B T_C}) - 1}] \\
&= I_{SC,ref} \frac{G}{G_{ref}} [1 - \alpha[T_{C,ref} - T_C]] [1 - \frac{\exp(\frac{qV_L}{nk_B T_C}) - 1}{\exp(\frac{qV_{OC}(G, T_C)}{nk_B T_C}) - 1}] \\
&= I_{SC,ref} \frac{G}{G_{ref}} [1 - \alpha[T_{C,ref} - T_C]] \\
&\quad * [1 + \frac{1 - \exp(\frac{qV_L}{nk_B T_C})}{1 - \exp(\frac{q[V_{OC,ref}[1 - \beta[T_{C,ref} - T_C]] + \frac{nk_B(T_{C,ref} + T_C/\gamma)}{q} \ln(\frac{G}{G_{ref}})]}{nk_B T_C}}]
\end{aligned} \tag{A} \quad (2.19)$$

See <https://www.desmos.com/calculator/yp0rhmbkz> to play around with the complete three parameter solar cell model. Add as a figure later on compared to experimental data.

2.2 Five Parameter Solar Cell Model

2.2.1 Model Introduction

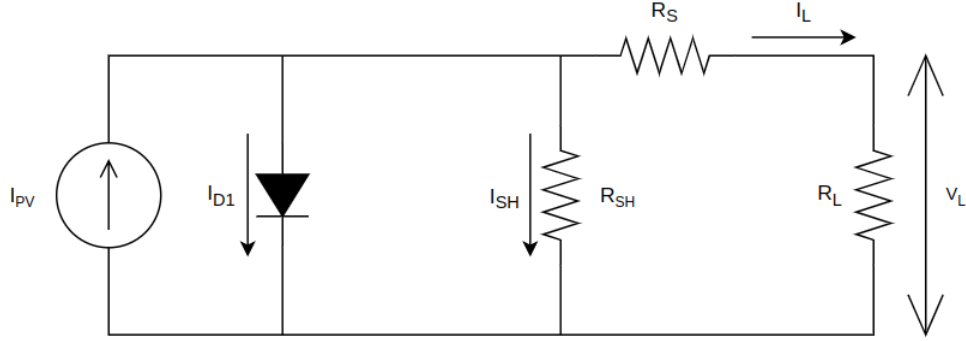


Figure 2.5: Five Parameter, or Full Single Diode Model of a Solar Cell

The most common model for solar cells is the five parameter solar cell model, shown in Figure 2.5. This is the complete form of the single diode model discussed in the previous section, Section 2.1. There are two added components/parameters: a series resistance R_S and shunt resistance R_{SH} , whose primary roles are to alter the shape of the knee-bend in the I-V curve. As such, this model improves upon the main flaw of the three parameter solar cell model, that of overshooting the maximum power point.

In the following subsections, we discuss the two added parameters and their specific effects on the model.

2.2.2 Shunt Resistance

As shown in Figure 2.6 (b) from Nelson [14], as the shunt resistance R_{SH} decreases, the top of the knee-bend of the I-V curve will be forced down. At low values of shunt resistance (on the order of $10\ \Omega$), the knee-bend will be pushed down so much that the curve becomes a straight line. At high values of shunt resistance, (on the order of $100\ \Omega$), the curve converges to some fixed maximum bend constrained by other parameters of the model. This relationship is generally considered logarithmic.

The shunt current (I_{SH}) can be added to the simple form of the model as a new term as shown in Equation 2.20. Assuming that the series resistance

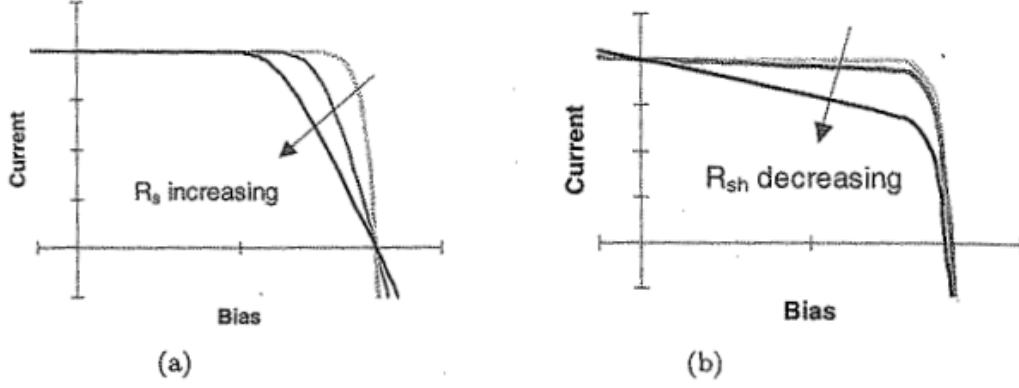


Figure 2.6: Effect of Series (a) and Shunt Resistance (b) on **I-V** Curve

is negligible (0), we can determine that I_{SH} is a function of the R_{SH} and the voltage across the cell V_L , as shown in Equation 2.21.

$$I_L = I_{PV} - I_D - I_{SH} \quad (A) \quad (2.20)$$

$$I_L = I_{PV} - I_D - \frac{V_L}{R_{SH}} \quad (A) \quad (2.21)$$

2.2.3 Series Resistance

The series resistance R_S forces the knee-bend of the **I-V** curve to the left or right, as opposed to up and down for the shunt resistance. As the series resistance increases, more current is consumed across the lumped resistance before reaching the terminals of the solar cell, reducing the expected current in the curve as shown in Figure 2.6 (a). At high values of series resistance, the curve likewise becomes a straight line.

The series resistance R_S term impacts the consumers of the five parameter solar cell model; namely the dark current and the shunt resistance terms. A visualization of this is shown as Figure 2.7.

Revisiting Equation 2.4, we know that the dark current depends on the voltage across the cell V_L generated by the load current I_L flowing through the load resistance load resistance (R_L) connected at the cell terminals. This allows us to reformulate the dark current equation as Equation 2.22. Here, we add the voltage drop across the lumped series resistance summed with the

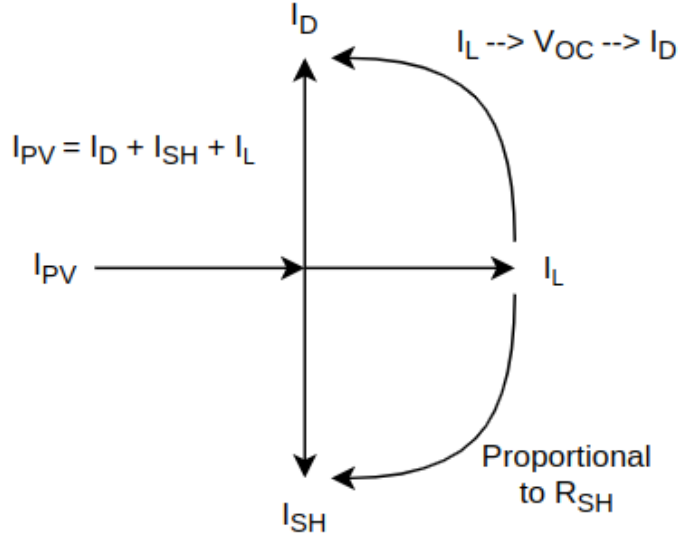


Figure 2.7: Current Flow Junction of Five Parameter Model Solar Cell

load voltage V_L to represent the total voltage expected by the dark current model.

$$I_D = I_0 \left[\exp\left(\frac{V_L + I_L R_S}{V_T}\right) - 1 \right] \quad (\text{A}) \quad (2.22)$$

We can likewise use the voltage drop to update the shunt resistance term, shown in Equation 2.23.

$$I_{SH} = \frac{V_L + I_L R_S}{R_{SH}} \quad (\text{A}) \quad (2.23)$$

Combining these two effects, we form Equation 2.24.

$$I_L = I_{PV} - I_0 \left[\exp\left(\frac{V_L + I_L R_S}{V_T}\right) - 1 \right] - \frac{V_L + I_L R_S}{R_{SH}} \quad (\text{A}) \quad (2.24)$$

We note that this model is an implicit function and cannot easily (or prettily) move all the I_L terms to the left side of the equation. As such, for these types of problems, we will develop and use iterative solvers to determine I_L for a given set of input parameters (R_S , G , V_L , etc). Iterative solvers involve starting with a guess for the output parameter (in this case I_L) and

attempt to improve upon that guess such that each side is equal to each other or within some tolerance to each other. An in depth discussion on how these solvers were implemented for this model and variants of this model can be found in Appendix C.

2.2.4 Photocurrent as a Ratio of Shunt/Series Resistance

An interesting addition to the five parameter cell model is presented by Cubas et al [3][4]: they observe that Equation 2.24 in short circuit conditions results in Equation 2.25.

$$I_{SC} = I_{PV} - I_0[\exp(\frac{I_{SC}R_S}{V_T}) - 1] - \frac{I_{SC}R_S}{R_{SH}} \quad (A) \quad (2.25)$$

In their analysis of measurements taken across a broad spectrum of reference solar cells, represented in Table 2.2, the dark current at short circuit conditions were well less than a single milliampere, an insignificant fraction of the total operating current. From this observation Cubas et al. rewrites the above expression to get the photocurrent as a function of the short circuit current and a ratio of the series and shunt resistance, shown in Equation 2.26.

$$I_{PV} = I_{SC} \frac{R_S + R_{SH}}{R_{SH}} \quad (A) \quad (2.26)$$

Reference	Cell Type	I_{SC} (A)	$I_0[e^{\frac{I_{SC}R_S}{V_T}} - 1]$ (A)	I_D / I_{SC}
Kennerud, 1969	CdS	0.8040	1.56E-5	1.94E-5
Charles, 1981	BSC	0.1023	2.21E-8	2.16E-7
Charles, 1981	GSC	0.5610	1.01E-5	1.80E-5
Lo Brano, 2010	Q6LM	7.6650	1.42E-9	1.85E-10

Table 2.2: Dark Current Ratios for Various Reference Cells

However, a cursory evaluation of the parameter space (V_{OC} , I_{SC} , G , T_C , R_S , n) reveals that the assumption that the dark current is negligible breaks down when a subset of the following conditions occur:

- the open circuit voltage V_{OC} becomes very small,
- the short circuit current I_{SC} becomes very large,
- and the series resistance R_S becomes relatively large for some combination of V_{OC} and I_{SC} .

Is it to be noted that these parameters are tightly coupled, and therefore the language specifying a parameter space upon which this term should be used remains imprecise. We also note that the temperature and ideality factor when increased slightly tighten the viable parameter space.

However, when considering a specific solar cell that is *appropriate* (e.g. it contains **STC** defined parameters V_{OC} and I_{SC} with an measured R_S that results negligible I_D), this term remains negligible unless the cell is exposed to (1) high temperatures or (2) high intensity light, two conditions that tend to come hand in hand. These conditions tend to only be experienced by concentrator photovoltaics and are highly unlikely to be reached by normal solar cells.

We will observe later in Section 2.6 that with our dataset of Maxeon Gen III Bin Le1 solar cells, the vast majority of estimated series resistance is well below 0.08Ω , which results in dark currents less than a mA. This means that this modification (assuming it improves the accuracy of the model), is well suited for our solar cells.

Incorporating this revision, we arrive at Equation 2.27.

$$I_L = I_{SC} \frac{R_S + R_{SH}}{R_{SH}} - I_0 \left[\exp\left(\frac{V_L + I_L R_S}{V_T}\right) - 1 \right] - \frac{V_L + I_L R_S}{R_{SH}} \quad (\text{A}) \quad (2.27)$$

See <https://www.desmos.com/calculator/nniw0mha2k> to play around with the revised dark current model. Add as a figure later on compared to experimental data.

2.2.5 Shunt and Series Resistance as a Function of Irradiance, Temperature

Throughout this major section, we introduced the notion of shunt and series resistance as internal parasitics. However, we did not explore whether these ‘internal parameters’ are themselves affected by external conditions such as irradiance and temperature.

A comprehensive review and experimental paper from F  bba et al [5] performed experiments on solar cells to evaluate the effect of temperature and irradiance on shunt and series resistance, controlling for the two independent variables in ranges of 25  C to 55  C and 600W/m  2 to 1000W/m  2, respectively. Four figures, Figures 2.8 - 2.11 are shown below to illustrate the following assertions.

For shunt resistance, they observed the following trends:

- as temperature increases, the shunt resistance exponentially decays,
- and as irradiance increases, the shunt resistance linearly decreases.

For series resistance, they observed the following trends:

- as temperature increases, the series resistance exponentially decays,
- and as irradiance increases, the series resistance linearly increases.

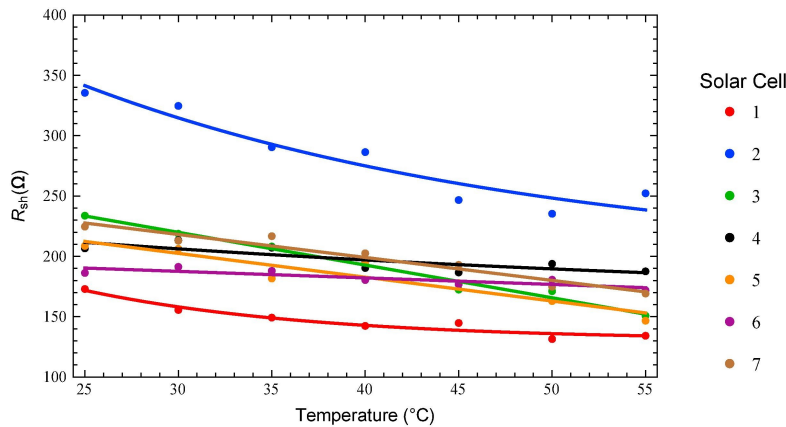


Figure 2.8: Shunt Resistance vs Temperature [5]

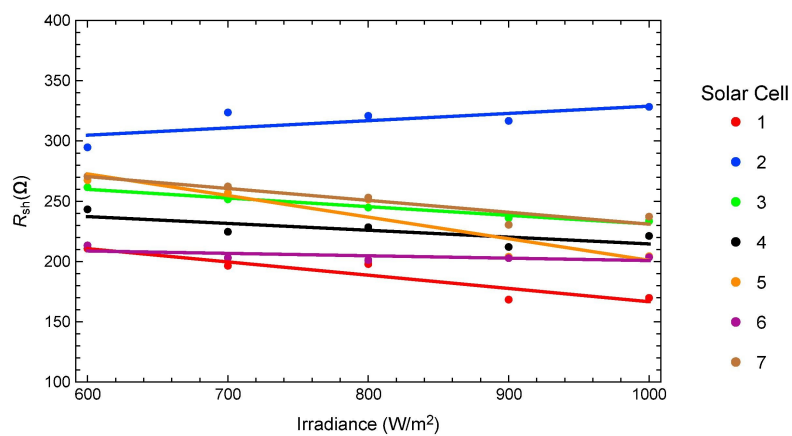


Figure 2.9: Shunt Resistance vs Irradiance [5]

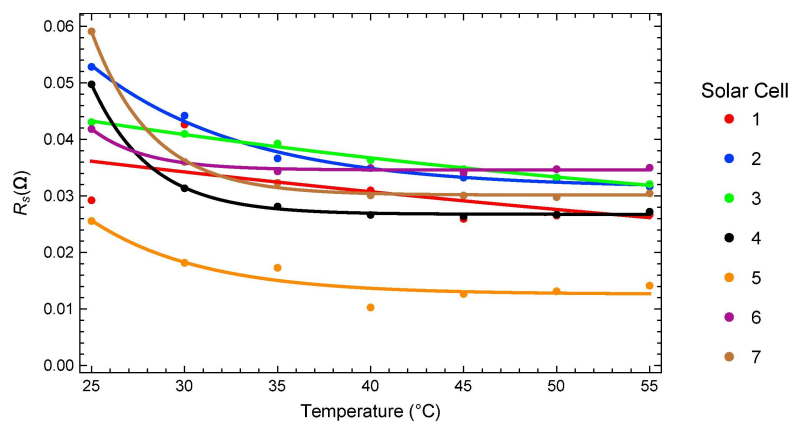


Figure 2.10: Series Resistance vs Temperature [5]

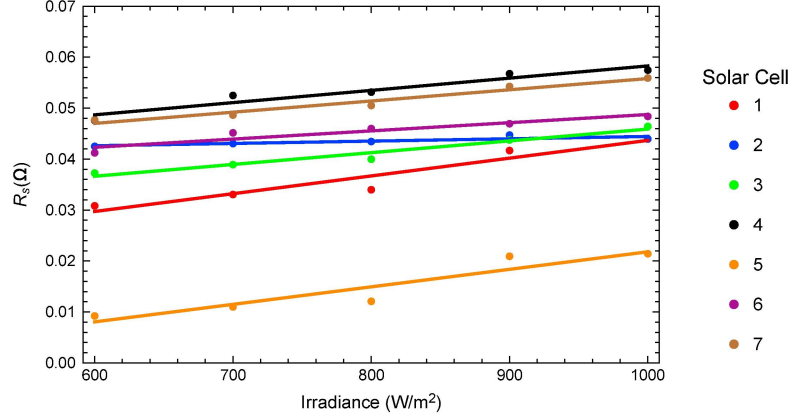


Figure 2.11: Series Resistance vs Irradiance [5]

Fébba et al. did not posit a revised model of the either resistance term (although they did provide explanations on why the trends were reasonable), but Baig et al. [1] and MacAlpine et Brandemuehl [10] introduced a variant of Equation 2.28, where ζ is a new temperature coefficient.

$$R_S = R_{S,ref} \exp(\zeta[T_{C,ref} - T_C]) \quad (\Omega) \quad (2.28)$$

We extend Fébba et al [5]'s results to generate Equation 2.29, where η is applied to Equation 2.28 as a new irradiance coefficient.

$$R_S = R_{S,ref} \exp(\zeta[T_{C,ref} - T_C])[1 + \eta(G - G_{ref})] \quad (\Omega) \quad (2.29)$$

We also propose Equation 2.30 to model the shunt resistance, where κ is a new temperature coefficient and ι is a new irradiance coefficient.

$$R_{SH} = R_{S,ref} \exp(\kappa[T_{C,ref} - T_C])[1 - \iota(G - G_{ref})] \quad (\Omega) \quad (2.30)$$

We also note that a solar cell consists of a network of resistors and diodes. If we dispel the assumptions that the solar cell is (a) entirely and evenly illuminated, (b) uniformly heated, and (c) of consistent manufacturing quality, the apparent series resistance measured at the terminals of the cell can fluctuate. An example of this is provided below in Figure 2.12. Depending on the proportion of the solar cell with varying amounts of series resistance, the observed I-V curve could differ greatly.

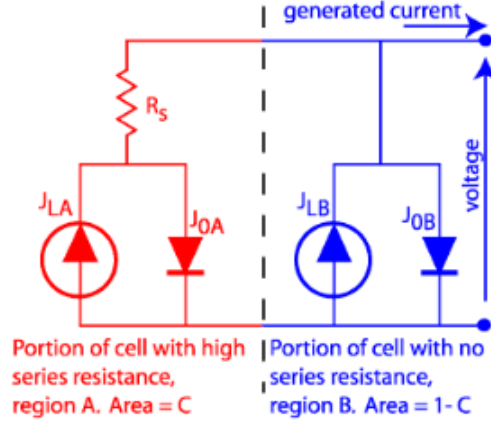


Figure 2.12: Solar Cell With Varying Series Resistances [13]

Replication of F  bba et al’s work is presented in Appendix D, where a custom testbed is used to measure solar cell curves at various temperature and irradiance levels at a broader range compared to F  bba et al (0°C to 100°C and $0\text{W}/\text{m}^2$ to $1000\text{W}/\text{m}^2$, respectively). Additionally, Appendix D also discusses methods to evaluate the resistances and their respective coefficients. The evaluation of the effectiveness of these terms in predicting the expected I - V curves warrants their own subsection in Section 2.4.

2.2.6 Model Summary

To conclude this major section, we will review the components that make up the five parameter cell model, propose an item of further exploration, and propose a complete model function that incorporates the topics discussed.

Firstly, the five parameter cell model retains the attributes of the three parameter cell model, being the complete form of the single diode model. It adds two parameters, a shunt resistance R_{SH} and series resistance R_S that represent ohmic losses in the solar cell, which primarily affect the knee-bend of the resultant I - V curve. These two parameters help reduce error in the model around the knee-bend that cannot fully be represented by the ideality factor. However, these additions increase the complexity of the model, and the resultant form is an implicit equation that requires an iterative solver approach.

Secondly, we investigate a revision to the photocurrent model to make

it also a function of the shunt and series resistance. This was obtained by evaluating the short circuit condition of the existing model and reducing the dark current term under appropriate conditions. We note that this new model may not work under specific conditions, namely for concentrator solar cells or for solar cells with inordinately large series resistance relative to their specific V_{OC} and I_{SC} combination.

We also discuss evaluating the shunt and series resistance themselves as a function of temperature and irradiance. We observe that these values tend to have exponential relationships with temperature and linear relationships with irradiance, although we require further data to validate the strength of these correlations. We derive initial models for these parameters, and discuss real world conditions in which they might deviate from our expectations (e.g. partial shading).

As such, we will revisit both of these modifications to the base model in a further section to prove or disprove their veracity and usefulness to the overall model.

Finally, we incorporate these changes into the complete function defined in the previous section. This is presented as Equation 2.31 (I_{SC} , V_{OC} , R_S , R_{SH} , and V_T abstracted out for clarity and brevity).

Reformat
this
equation

$$\begin{aligned}
 I_L(V_L, G, T_C) &= I_{PV}(G, T_C, R_S, R_{SH}) - I_D(V_L, G, T_C, R_S) - I_{SH}(R_S, R_{SH}) \\
 &= I_{SC}(G, T_C) \frac{R_S + R_{SH}}{R_{SH}} - I_0(G, T_C) \left[\exp\left(\frac{V_L + I_L R_S}{V_T(T_C)}\right) - 1 \right] - \frac{V_L + I_L R_S}{R_{SH}} \\
 &= I_{SC}(G, T_C) \frac{R_S + R_{SH}}{R_{SH}} - I_{SC}(G, T_C) \frac{\exp\left(\frac{V_L + I_L R_S}{V_T(T_C)}\right) - 1}{\exp\left(\frac{V_{OC}(G, T_C)}{V_T(T_C)}\right) - 1} - \frac{V_L + I_L R_S}{R_{SH}} \\
 &= I_{SC}(G, T_C) \left[\frac{R_S + R_{SH}}{R_{SH}} + \frac{1 - \exp\left(\frac{V_L + I_L R_S}{V_T(T_C)}\right)}{1 - \exp\left(1 - \frac{V_{OC}(G, T_C)}{V_T(T_C)}\right)} \right] - \frac{V_L + I_L R_S}{R_{SH}}
 \end{aligned}
 \tag{A} \quad (2.31)$$

See <https://www.desmos.com/calculator/yp0rhmbkz> to play around with the complete three parameter solar cell model. Add as a figure later on compared to experimental data.

2.3 Seven Parameter Solar Cell Model

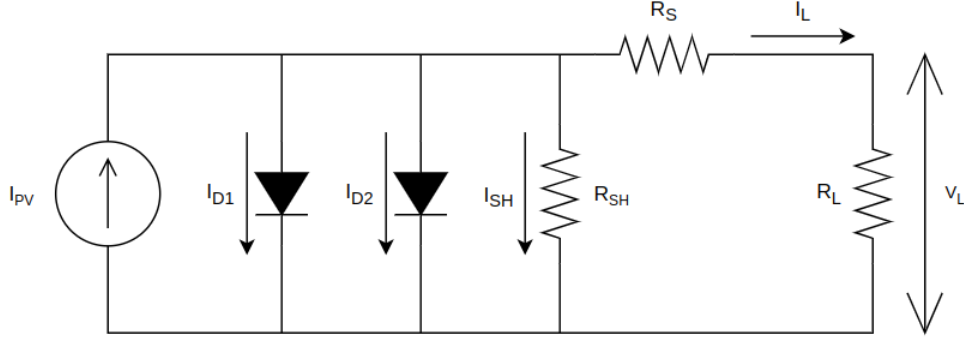


Figure 2.13: Seven Parameter, or Double Diode Model of a Solar Cell

The seven parameter solar cell model, also known as a double diode model, shown in Figure 2.13, builds upon the five parameter model by introducing a second diode (hence the name) to more accurately model internal current losses, which can be split into the following:

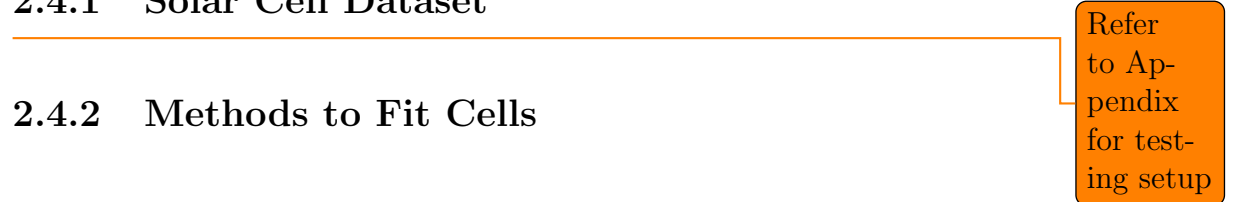
- losses due to carrier recombination in the space charge region of the P-N junction,
- and losses due to surface recombination.

These currents are denoted the carrier recombination dark current (I_{D1}) and surface recombination dark current (I_{D2}), respectively. By differentiating between the two primary recombination processes in the cell, the seven parameter model is generally considered more accurate than the five parameter model.

2.4 Evaluation of Solar Cell Models

2.4.1 Solar Cell Dataset

2.4.2 Methods to Fit Cells



Refer
to Ap-
pendix
for test-
ing setup

2.5 Modeling Solar Modules

2.6 Evaluation of Solar Module Models

2.7 Modeling Solar Arrays

2.8 Evaluation of Solar Array Models

...

Insert
conclu-
sion on
chapter
topics
and re-
sults.

Chapter 3

Optimizing Photovoltaics

Insert intro paragraph on the focus of this chapter, as well as the a short discussion of the following sections.

Insert conclusion on chapter topics and results.

Chapter 4

Optimizing Photovoltaic Systems

Insert intro paragraph on the focus of this chapter, as well as the a short discussion of the following sections.

Insert sankey diagram from incident light to battery input

Insert conclusion on chapter topics and results.

Chapter 5

Conclusion

Bibliography

- [1] Mirza Qutab Baig, Hassan Abbas Khan, and Syed Muhammad Ahsan. “Evaluation of solar module equivalent models under real operating conditions—A review”. In: *Journal of Renewable and Sustainable Energy* 12.1 (2020), p. 012701. DOI: [10.1063/1.5099557](https://doi.org/10.1063/1.5099557). eprint: <https://doi.org/10.1063/1.5099557>. URL: <https://doi.org/10.1063/1.5099557>.
- [2] M. Chegaar et al. “Effect of Illumination Intensity on Solar Cells Parameters”. In: *Energy Procedia* 36 (2013). TerraGreen 13 International Conference 2013 - Advancements in Renewable Energy and Clean Environment, pp. 722–729. ISSN: 1876-6102. DOI: <https://doi.org/10.1016/j.egypro.2013.07.084>. URL: <https://www.sciencedirect.com/science/article/pii/S1876610213011703>.
- [3] Javier Cubas, Santiago Pindado, and Carlos Manuel. “Explicit Expressions for Solar Panel Equivalent Circuit Parameters Based on Analytical Formulation and the Lambert W-Function”. In: *Energies* 7 (June 2014), pp. 4098–4115. DOI: [10.3390/en7074098](https://doi.org/10.3390/en7074098).
- [4] Javier Cubas, Santiago Pindado, and Marta Victoria. “On the analytical approach for modeling photovoltaic systems behavior”. In: *Journal of Power Sources* 247 (2014), pp. 467–474. ISSN: 0378-7753. DOI: <https://doi.org/10.1016/j.jpowsour.2013.09.008>. URL: <https://www.sciencedirect.com/science/article/pii/S0378775313014997>.
- [5] D.M. Fébba et al. “Impacts of temperature and irradiance on polycrystalline silicon solar cells parameters”. In: *Solar Energy* 174 (2018), pp. 628–639. ISSN: 0038-092X. DOI: <https://doi.org/10.1016/j.solener.2018.09.051>. URL: <https://www.sciencedirect.com/science/article/pii/S0038092X18309435>.

- [6] R.N. Hall. “Silicon photovoltaic cells”. In: *Solid-State Electronics* 24.7 (1981), pp. 595–616. ISSN: 0038-1101. DOI: [https://doi.org/10.1016/0038-1101\(81\)90188-X](https://doi.org/10.1016/0038-1101(81)90188-X). URL: <https://www.sciencedirect.com/science/article/pii/003811018190188X>.
- [7] Yoshihiro Hishikawa et al. “Temperature dependence of the short circuit current and spectral responsivity of various kinds of crystalline silicon photovoltaic devices”. In: *Japanese Journal of Applied Physics* 57.8S3 (July 2018), 08RG17. DOI: [10.7567/JJAP.57.08RG17](https://doi.org/10.7567/JJAP.57.08RG17). URL: <https://dx.doi.org/10.7567/JJAP.57.08RG17>.
- [8] *Ideality factor*. PVEducation. URL: <https://www.pveducation.org/pvcdrom/solar-cell-operation/ideality-factor#:~:text=The%20ideality%20factor%20of%20a,certain%20assumptions%20about%20the%20cell>.
- [9] Amit Jain and Avinashi Kapoor. “A new method to determine the diode ideality factor of real solar cell using Lambert W-function”. In: *Solar Energy Materials and Solar Cells* 85.3 (2005), pp. 391–396. ISSN: 0927-0248. DOI: <https://doi.org/10.1016/j.solmat.2004.05.022>. URL: <https://www.sciencedirect.com/science/article/pii/S0927024804002442>.
- [10] Sara M. MacAlpine and Michael J. Brandemuehl. “Photovoltaic module model accuracy at varying light levels and its effect on predicted annual energy output”. In: *2011 37th IEEE Photovoltaic Specialists Conference*. 2011, pp. 002894–002899. DOI: [10.1109/PVSC.2011.6186551](https://doi.org/10.1109/PVSC.2011.6186551).
- [11] Gaetan Masson et al. *Snapshot of Global PV Markets 2022 Task 1 Strategic PV Analysis and Outreach PVPS*. Apr. 2022. ISBN: 978-3-907281-31-4.
- [12] Gaetan Masson et al. *Trends in Photovoltaic Applications 2022*. Oct. 2022. ISBN: 978-3-907281-35-2.
- [13] *Measurement of Series Resistance*. PVEducation. URL: <https://www.pveducation.org/pvcdrom/characterisation/measurement-of-series-resistance>.
- [14] Jenny Nelson. “Introduction”. In: *The physics of Solar Cells*. Imperial College Press, 2013, p. 14.
- [15] *Net Zero by 2050*. Paris: IEA Photovoltaic Power Systems Programme, 2021.

- [16] United Nations Environment Programme. *Paris Agreement*. 12/12/2015. URL: <https://wedocs.unep.org/20.500.11822/20830>.
- [17] Dani Rusirawan and István Farkas. “Identification of Model Parameters of the Photovoltaic Solar Cells”. In: *Energy Procedia* 57 (2014). 2013 ISES Solar World Congress, pp. 39–46. ISSN: 1876-6102. DOI: <https://doi.org/10.1016/j.egypro.2014.10.006>. URL: <https://www.sciencedirect.com/science/article/pii/S1876610214013733>.
- [18] Brady Tyra et al. *Electric Power Monthly*. U.S. Energy Information Administration, Oct. 2022. URL: <https://www.eia.gov/electricity/monthly/archive/october2022.pdf>.

Appendices

Appendix A

Acronyms and Abbreviations

BPS	battery protection system
EIA	U.S. Energy Information Administration
GW	Gigawatts
IEA	International Energy Association
I-V	current-voltage
LHRs	Longhorn Racing Solar
MPPT	maximum power point tracking
PV	photovoltaic
P-V	power-voltage
STC	standard test conditions
UN	United Nations

Appendix B

Mathematical Nomenclature

A area

$b_S(E)$ spectral photon flux density

E energy

G irradiance

I_L load current

I_D dark current, or diode current

I_{D1} carrier recombination dark current

I_{D2} surface recombination dark current

I_{PV} photocurrent, or light generated current

I_S series current

I_{SC} short circuit current

I_{SH} shunt current

I_0 dark saturation current, or reverse saturation current

K_B Boltzmann constant

K_E short circuit current constant

n ideality factor

$QE(E)$ quantum efficiency

q electric charge constant

R_L load resistance

R_S series resistance

R_{SH} shunt resistance

T_C cell temperature

V_L load voltage

V_T thermal voltage

V_{OC} open circuit voltage

Appendix C

Iterative Solvers for the Five Parameter Solar Cell Model

Appendix D

Measurement of Parasitic Resistances

TODOS

■ The second area of development may be more generalized then this.	6
■ Insert intro paragraph on the focus of this chapter, as well as the a short discussion of the following sections.	8
■ Reformat this equation	17
■ See https://www.desmos.com/calculator/yp0rhmabkz to play around with the complete three parameter solar cell model. Add as a figure later on compared to experimental data.	18
■ See https://www.desmos.com/calculator/nniw0mha2k to play around with the revised dark current model. Add as a figure later on compared to experimental data.	23
■ Reformat this equation	28
■ See https://www.desmos.com/calculator/yp0rhmabkz to play around with the complete three parameter solar cell model. Add as a figure later on compared to experimental data.	28
■ Refer to Appendix for testing setup	30
■ Insert conclusion on chapter topics and results.	34
■ Insert intro paragraph on the focus of this chapter, as well as the a short discussion of the following sections.	35
■ Insert conclusion on chapter topics and results.	35
■ Insert intro paragraph on the focus of this chapter, as well as the a short discussion of the following sections.	36
■ Insert sankey diagram from incident light to battery input	36
■ Insert conclusion on chapter topics and results.	36